JOURNAL OF SOLID STATE CHEMISTRY **132,** 60–72 (1997)
ARTICLE NO. SC977409

Crystal Structures of Ru Complex Sensitizers of TiO_2 Anatase Nanopowders

V. Shklover[1] and T. Haibach

Laboratory of Crystallography, Swiss Federal Institute of Technology, CH-8092 Zürich, Switzerland

B. Bolliger, M. Hochstrasser, M. Erbudak, and H.-U. Nissen

Institute of Solid State Physics, Swiss Federal Institute of Technology, CH-8093 Zürich, Switzerland

and

S. M. Zakeeruddin, Md. K. Nazeeruddin, and M. Grätzel

Laboratory for Photonics and Interfaces, Institute of Physical Chemistry, Swiss Federal Institute of Technology, CH-1015 Lausanne, Switzerland

Received October 9, 1996; in revised form March 31, 1997; accepted April 3, 1997

The crystal structure of a new Ru complex sensitizer is determined ($C_{29}H_{30}N_5O_4S_2Ru$, monoclinic, space group $P2_1/b$, $a = 11.400(4)$, $b = 15.236(6)$, $c = 18.748(7)$ Å, $\gamma = 85.17(3)^\circ$, $Z = 4$). The crystal structure of three efficient Ru sensitizers of TiO_2 anatase nanocrystalline powders are discussed in terms of formation of two-dimensional molecular packing which could also exist on the dye-coated anatase surfaces. The surface areas of sensitizers on the flat semiconductor surface are determined. The atomic structure of the (001) and (101) surface of naturally grown TiO_2 anatase have been investigated using low-energy electron diffraction (LEED) and the technique of secondary-electron imaging (SEI). The structure of both surfaces is found to be very sensitive to external physical influences; even a mild sputtering with He^+ ions results in a destruction of the surface structure in several atomic layers. The anatase surface was found to be covered with less than one atomic layer thicker contamination. The results of LEED and SEI studies could be well reproduced by model calculation based on the atomic structure of nonreconstructed surface. Thus, it is concluded that the bulk crystalline structure of naturally grown anatase continues up to the surface without modification. The first results on the orientation of sensitizer molecules on the mostly exposed surface (101) of anatase single crystal are obtained from HRTEM data. The amount of sensitizer molecules on the mostly exposed faces of anatase nanocrystals in thin colloidal TiO_2 anatase films could be estimated using crystal structural data of both the sensitizer and the anatase surface.

INTRODUCTION

Polypyridine complexes of Ru(II) have been extensively used as a photosensitizers in photovoltaic cells based on porous nanocrystalline TiO_2 (anatase) electrodes (1). The efficiency of the sensitization is determined, by the electron injection from a photoexcited state of the dye into the conduction band of the semiconductor (2). This interfacial electron transfer processes depends on number of factors: (a) the excited state should have thermodynamically enough driving force to inject electrons into the conduction band; (b) the oxidized sensitizer should be stable, in order to capture the dye localized hole by electron donor in solution; (c) transport of the injected electron to an external circuit; (d) rate of back electron transfer; and (e) surface density of sensitizer molecules, forming monomolecular layers on the mostly exposed faces of the anatase nanocrystals (faces (101) and (001)) (3). The sensitizer surface density may be estimated from the known molecular and crystal structure of the sensitizer or its precursor. The structural studies of composite (layered) organic/inorganic structures may enable the direct consideration of the structure of organic/inorganic interface, including (a) structure of organic frontier layer and (b) geometry of bonding between organic and inorganic parts. For example, the structural study of layered organic/inorganic crystals of merocyanine dye (4) has shown that significant change of important characteristics of one (organic) partial structure (shift of absorption band) may be achieved by a small variation of the other (inorganic) part. The study of composite structures of 2-amino-5-nitropyridinium in different inorganic matrices (5–7) allowed the

[1] To whom correspondence should be addressed.

0022-4596/97 $25.00

induction of (nonlinear optical) designed composite properties of structure by modification of organic and/or inorganic components. The polar crystal symmetry of the inorganic part was induced by symmetry and alignment of molecules in the organic part, the charge-transfer properties of which were influenced by the inorganic component.

In this work we aimed to compare the crystal packing properties of three efficient photosensitizers on nanocrystalline TiO_2 (anatase) powders. The three ruthenium-based photosensitizers are [bis(4,4′-dicarboxy-2,2′-bipyridine)bis (thiocyanato)]ruthenium(II) (**1**), 4-phosphonato-(2,2′; 6,2″-terpyridine)(4,4′-dimethyl-2,2′-bipyridine)(thiocyanato) ruthenium(II) (**2**), and (4,4′-dicarboxy-2,2′-bipyridine) (4,4′-dimethyl-2,2′-bipyridine)(*N*,*N*-diethyldithiocarbamato)ruthenium(II) (**3**). The single crystals of sensitizer **2** suitable for X-ray study, obtained from a DMSO solution, are abbreviated as **2a**, and **2** used for the anatase single crystal coating and for powder diffraction is abbreviated as **2b**. The structures of complexes **1** and **2** were reported earlier (3, 8). In this work we report the structure of sensitizer **3**.

The electron microscopy TEM and SEM studies on colloidal TiO_2 films have shown that the (101) are the most exposed faces of nanocrystals (3). Nevertheless, the possible chemical and physical surface reconstruction of (nano)crystals should be taken into account, before considering the structural interrelation between the structures of organic coating and inorganic matrix (9). That is why the atomic structure of TiO_2 anatase has been investigated with the low-energy electron diffraction (LEED) (10) and secondary-electron imaging (SEI) techniques, using naturally grown anatase single crystal.

X-RAY STRUCTURE DETERMINATION OF SENSITIZER 3

Synthesis of sensitizer **3** is described in detail (11). Crystal data and details of the X-ray structure determination of **3** are given in Table 1. The data collection for the plate-like single crystal **3** was performed at 210 K (because of very small size and instability of crystals due to the loss of solvent molecules) on an Enraf–Nonius CAD-4 diffractometer using Mo$K\alpha$ radiation ($\lambda = 0.71073$ Å) equipped with a graphite monochromator. Using $w/2\Theta$ scan technique all reflections in the range $2^\circ < 2\Theta < 45.94^\circ$ were collected using CAD-4-EXPRESS software (12). The index ranges were $-12 < h < 12$, $0 < k < 16$, $-20 < l < 20$. Three standard reflections were measured every 1 hour for the intensity control and two standard reflections were checked every 100 reflections for the orientational control. The intensities were measured with a prescan-determined scan speed to reach the ratio $s(I)/I = 0.03$, the maximum measurement time was 30 sec per reflection, individual scan range $\Delta\omega = (1.16 - 1.42 + 0.78 \tan\Theta)^\circ$, $\Delta\psi = (3.57 - 4.42 + 1.42 \tan\Theta)$ mm. For the absorption correction, ψ-scan of 9 reflections with the step $\Delta\psi = 10^\circ$ was performed. The minimum and maximum transmission coefficients were 86.25 and 99.89%, respectively. Structure **3** was solved by direct methods. In difference Fourier synthesis it was found that crystal **3** contains crystallization water molecule. In consequence, the composition of crystal **3** is $C_{29}H_{30}N_5O_4S_2Ru \cdot H_2O$. The structure was refined by full-matrix least-squares with anisotropic displacement parameters for the atoms Ru, S, O, and all atoms of terminal methyl, acetyl and dithiocarbamate groups. The H atoms in complex **3** were placed in the idealized positions and used in the calculation of the structure factors (riding model). The hydrogen atoms of water molecules were not localized. Experimental details and results of the structure refinement are summarized in Table 1; the atomic coordinates are given in Table 2. Programs of the SHELXTL PLUS were used for data reduction, structure solution and refinement (13). Additional materials are available from NAPS.[2]

TABLE 1
Experimental Details of the X-Ray Structure Determination of Crystal 3

Chemical formula	$C_{29}H_{30}N_5O_4S_2Ru \cdot H_2O$
Formula weight	691.3
Crystal color, habit	Brown, plate
Crystal dimensions (mm)	$0.1 \times 0.2 \times 0.3$
Crystal system	Monoclinic
Lattice parameters	
a (Å)	11.400(4)
b (Å)	15.236(6)
c (Å)	18.748(7)
γ (°)	85.17(3)
V (Å^3)	3245(1)
Space group	$P2_1/b$
Z	4
Density calc. (mg · m^{-3})	1.415
Absorption coefficient (Mo$K\alpha$) (mm^{-1})	0.655
F(000)	1428
T (K)	293
2Θ range (°)	2–45.94
Reflection measured	20750
Independent reflections	4508
R_{int}	0.060
Observed reflections ($F - 4s(F)$)	1448
Number of refined parameters	259
Residuals R, R_w	0.078, 0.083
Reflections/parameters ratio	5.01/1
Goodness of fit	1.03
Largest residual electron density ($e \cdot$ Å^3)	1.22
Largest difference hole ($e \cdot$ Å^3)	0.55

[2]See NAPS document No. 05404 for 31 pages of supplementary material. This is not a multi-article document. Order from NAPS c/o Microfiche Publications, P.O. Box 3513, Grand Central Station, New York, NY 10163-3513. Remit in advance in U.S. funds only $7.75 for photocopies or $5.00 for microfiche. There is a $15.00 invoicing charge on all orders filled before payment. Outside U.S. and Canada add postage of $4.50 for the first 20 pages and $1.00 for each 10 pages of material thereafter, or $1.75 for the first microfiche and $.50 for each microfiche thereafter.

TABLE 2

Atomic Coordinates ($\times 10^4$ for Ru and S, $\times 10^3$ for O, N, and C Atoms) and Equivalent Isotropic Displacement Parameters B_{eq} (Å^2, $\times 10^3$ for Ru and S, $\times 10^2$ for O, N, and C Atoms) for Crystal 3

Atom	x	y	z	B_{eq}
Ru(1)	346(2)	2523(1)	4780(1)	55(1)
S(1)	214(6)	3339(4)	4465(4)	66(3)
S(2)	996(6)	1939(4)	3683(4)	70(3)
O(31)	−366(2)	−60(2)	636(2)	25(3)
O(32)	−482(2)	15(1)	590(1)	14(1)
O(41)	171(1)	−107(1)	680(1)	8(1)
O(42)	351(1)	−56(1)	661(1)	9(1)
N(1)	−2(1)	329(1)	565(1)	50(5)
N(2)	−67(2)	341(1)	431(1)	56(6)
N(3)	−107(2)	165(1)	507(1)	49(6)
N(4)	111(1)	160(1)	535(1)	47(6)
N(9)	309(2)	276(1)	329(1)	9(1)
C(11)	−76(2)	392(1)	545(1)	37(6)
C(12)	−110(2)	447(1)	601(1)	42(6)
C(13)	−68(2)	442(2)	670(1)	56(7)
C(14)	3(2)	378(2)	684(1)	76(9)
C(15)	33(2)	327(1)	631(1)	58(8)
C(21)	−113(2)	399(1)	476(1)	49(7)
C(22)	−197(2)	458(1)	451(1)	66(8)
C(23)	−228(2)	454(1)	378(1)	61(8)
C(24)	−181(2)	397(1)	334(1)	62(8)
C(25)	−101(2)	343(2)	364(1)	67(8)
C(31)	−81(2)	98(1)	548(1)	32(6)
C(32)	−170(2)	41(1)	578(1)	49(7)
C(33)	−286(2)	53(1)	561(1)	48(7)
C(34)	−315(2)	123(1)	518(1)	49(7)
C(35)	−218(2)	175(1)	491(1)	45(7)
C(41)	42(2)	91(1)	562(1)	48(7)
C(42)	84(2)	24(1)	600(1)	34(6)
C(43)	199(2)	21(1)	612(1)	47(7)
C(44)	274(2)	92(1)	588(1)	75(9)
C(45)	226(2)	159(1)	548(1)	63(8)
C(16)	−110(2)	545(2)	707(1)	8(1)
C(26)	−318(3)	520(2)	353(2)	11(2)
C(36)	−383(3)	−4(2)	599(2)	10(2)
C(46)	247(2)	−54(1)	655(1)	6(1)
C(1)	223(3)	267(1)	373(1)	7(1)
C(3)	416(3)	331(2)	340(2)	10(2)
C(4)	312(4)	218(3)	265(2)	13(2)
C(5)	503(4)	284(2)	390(3)	23(4)
C(6)	276(5)	257(3)	203(3)	21(4)
O(1W)	290(4)	−231(2)	−233(2)	25(2)

The powder diffraction pattern of sensitizer **2b** was recorded on a Scintag powder diffractometer with a Ge detector using Cu radiation.

LEED AND SEI STUDIES OF THE SURFACE OF TiO_2 ANATASE SINGLE CRYSTAL

The LEED method is extremely sensitive to the change of the surface atomic lattice owing to the relatively short mean free path of the electrons (14), which is used to generate the diffraction patterns in an energy range of 30–400 eV. The SEI, on the other hand, discloses the real space symmetry of the atomic arrangement in a near surface region of a solid (15). The SEI involves the excitation of the surface layer by electrons having an energy near 2000 eV and subsequent two-dimensional spherical recording of the back-scattered electrons with energy losses up to 5% of the primary-beam energy. In order to explain the processes involved in the SEI image formation, the following model was used: Primary electrons penetrate the solid and scattered elastically as well inelastically by the atoms at and below the surface. These atoms are considered to be point sources for the scattered electrons which are subsequently scattered again by the surrounding atoms. At kilo-electron-volt energies, elastic forward scattering is the dominant process. Therefore, the electrons which can escape the solid are predominantly those scattered by atoms near the source. Hence, the electrons are focused along the atomic rows defined by the source and the adjacent atoms and in this way produce bright spots on the collector screen for particular directions of escape. Consequently, the observed pattern represents a central projection of the real space atomic arrangement around each source, with many sources contributing incoherently to the pattern. Since a finite region near the surface is imaged, this technique is sensitive not only to the surface atoms, but also to atoms beneath the surface. Hence, the SEI offers the possibility of studying the structure of a solid which is covered with an atomically thin layer of contamination. Rotation of the sample relative to the display unit allows three-dimensional views of the solid, this is very valuable in the case of unknown structure. Since direct projection imaging is responsible for the formation of the pattern, its computational interpretation is straightforward. Alternatively, a single-scattering cluster calculation (SSC) can be applied for more realistic reproduction of experimental data (16). The combination of LEED and SEI gives information about the atomic structure of the surface, surface perfection and its reconstruction and relaxation, if present. A practical advantage of this combination is the fact that one can switch between LEED and SEI experiments just by changing the electron energy without any modification in the apparatus.

The measurements were made in an ultrahigh vacuum apparatus, described earlier (15). The large naturally grown anatase single crystal of square-bipyramidal habitus with the dimensions of $15 \times 15 \times 25$ mm was mounted on a revolving manipulator so that the (001) and (101) surfaces were accessible by the simple rotation of the sample holder by approximately 68°. Initially, no efforts were made to clean the crystal surface. The electron beam, used to generate the pattern, was focused on the specimen to a spot size of 0.2 mm. For LEED it was operated in the energy range of 30–500 eV; for SEI the electron energy was 2000 eV. The

electrons, which are back scattered quasielastically from the surface are made visible by a sphere-shaped display system which spans a solid angle of $\sim 105^{\circ}$. The specimen was located in the center of the display system, and the primary electrons were incident along the axis of the sphere. Two concentrated grids were used to retard secondary electrons that have kinetic energy lower than about 95% of the primary energy and allow those with higher energies to contribute to pattern formation. The intensity contrast produced by the back-scattered electrons on the inner surface of the display sphere was recorded by a charge-coupled device camera within 2 sec.

SCANNING ELECTRON MICROSCOPY

The nanocrystalline colloidal powders of TiO_2 anatase were examined at 30 kV accelerating voltage in a Hitachi S-900 "in-lens" field-emission scanning electron microscope with a standard Everhard–Thornley SE detector and YAG-type BSE detector. Digital Micrograph 2.1 software was used for the digital processing of SEM images (17).

HIGH-RESOLUTION TRANSMISSION ELECTRON MICROSCOPY STUDY (HRTEM)

The HRTEM study of the TiO_2 anatase single crystals coated with **2b** sensitizer was performed at 300 kV on Philips CM 30 ST transmission electron microscope equipped with a detector for energy dispersive X-ray spectrometry (EDX) and a STEM attachment.

RESULTS AND DISCUSSION

One of the main requirements for an efficient sensitizer is having a spectral response in the red region in order to get maximum power. Toward this goal we made a molecular engineering to incorporate three different ligands in the same complex **3**. The aim of the synthesis of this complex is to create directionality in the excited state, so that on a photoexcitation the electron transfer should take place almost quantitatively. The details of the synthesis and electron injection efficiencies were reported elsewhere (11).

The hexacoordinated Ru atom has a distorted octahedral surrounding, because of the three different bidentate ligands. The similar geometry like in crystal **3** was observed in other structurally characterized ruthenium complexes (3, 8). The carboxylate ligand in complex **3** acts as a grafting unit onto the semiconductor surface providing the electronic coupling between the sensitizer and the semiconductor. In complex **3** diethyldithiocarbamate ligand coordinates to the ruthenium centre in a bidentate fashion. The purpose of introducing this ligand into the complex is to destabilize the metal t_{2g} orbital, thereby decreasing the gap between the highest occupied molecular orbital (HOMO) and the lowest unoccupied molecular orbital (LUMO). The electrochemical measurements of the complex shows that the LUMO of the 4,4′-dimethyl-2,2′-bipyridine is higher than the 4,4′-dicarboxy-2,2′-bipyridine. Hence in the excited state the electron is transferred to the 4,4′-carboxylate ligand which is in intimate contact with the conduction band of the TiO_2.

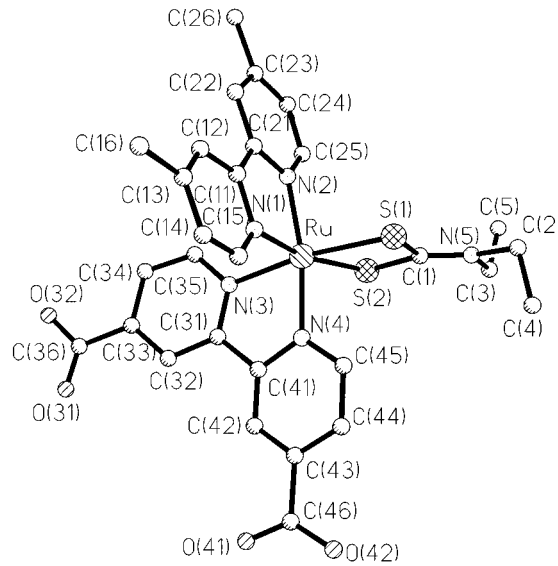

FIG. 1. Molecular structure of sensitizer **3**.

The molecular structure of the neutral complex **3** is shown in Fig. 1; the relevant bond distances and angles are given in the Table 3. The Ru–S distances are not equivalent, 2.376 and 2.383(6) Å, and are somewhat shorter than in the complex $[Ru(C_3H_6NS_2)(C_5H_5)(C_{18}H_{15}P)]$ as 2.394 and 2.397(3) Å (18). The increased values of the SRuN bond angles around the Ru atom draws attention, which constitute 91.8–96.0(5)°. The different values of bond angles S(1)RuN(4) and S(2)RuN(4) of 95.3(5) and 91.8(5)° may be explained by the different values of intramolecular contacts

TABLE 3
Bond Distances (Å) and Angles (°) around the Ru Atom in Structure 3

Ru(1)–S(1)	2.376(6)	Ru(1)–S(2)	2.383(7)
Ru(1)–N(1)	2.07(2)	Ru(1)–N(2)	2.05(2)
Ru(1)–N(3)	2.07(2)	Ru(1)–N(4)	2.02(2)
S(1)Ru(1)S(2)	72.6(2)	S(2)Ru(1)N(4)	91.8(5)
S(1)Ru(1)N(1)	96.0(5)	N(1)Ru(1)N(2)	79.46(7)
S(1)Ru(1)N(2)	93.4(5)	N(1)Ru(1)N(3)	88.7(7)
S(1)Ru(1)N(3)	171.4(5)	N(1)Ru(1)N(4)	95.4(7)
S(1)Ru(1)N(4)	95.3(5)	N(2)Ru(1)N(3)	94.6(7)
S(2)Ru(1)N(1)	167.1(5)	N(2)Ru(1)N(4)	170.3(7)
S(2)Ru(1)N(2)	94.9(6)	N(3)Ru(1)N(4)	77.0(7)
S(2)Ru(1)N(3)	103.4(5)		

C(45) ··· S(1) and C(45) ··· S(2) of 3.28(2) and 3.71(2) Å, respectively. In spite of the short C(45) ··· S(1) contact, the moiety RuS(1)S(2)C(1)N(5)C(2)C(3) retains in fact planar, maximum deviation is 0.08 Å. Nevertheless, some asymmetry still presents in the diethyldithiocarbamate ligand, the S(1) ··· C(3) and S(1) ··· C(5) separations somewhat exceed the corresponding S(2) ··· C(2) and S(2) ··· C(4) separations (3.05 and 3.60(2) Å and 3.10 and 3.71(2) Å, respectively). In the NMR time scale the diethyl groups of diethyldithiocarbamate are not chemically equivalent in solution (11). There are no specific intermolecular interactions of the lone pair of the N(5) atoms with the COOH groups in crystal **3**, which could serve as the reason for observed nonequivalence; the shortest contact of the N(5) atom with the oxygen atoms N(5) ··· O(31)(−1, −*y*, 1 − *z*) of 3.437 Å excludes such interaction. The non equivalence of the bond angles and bond distances may explain the observed differences in the chemical shifts of diethyl groups in the NMR spectrum or it could be due to the double bond nature of carbon nitrogen bond which is hindering the free rotation of ethyl groups around the nitrogen atom.

TABLE 4
Relevant Torsion Angles (°) in Complex 3

N(1)C(11)C(21)N(2)	178.2	N(3)C(31)C(41)N(4)	4.2
N(3)C(31)C(41)N(4)	4.2	C(32)C(33)C(36)O(31)	0.4
C(1)N(9)C(4)C(6)	99.2	C(32)C(33)C(36)O(32)	174.1
C(1)N(9)C(3)C(5)	80.2	C(42)C(43)C(46)O(41)	−4.4
N(1)C(11)C(21)N(2)	−1.1	C(42)C(43)C(46)O(42)	175.1

The π-delocalization between the COOH groups and the corresponding bipyridine moieties could be clearly seen from their coplanarity (Table 4); this is essential for the consideration of the location and electron transfer of sensitizer **3** on the semiconductor surface. Crystal **3** is built up of

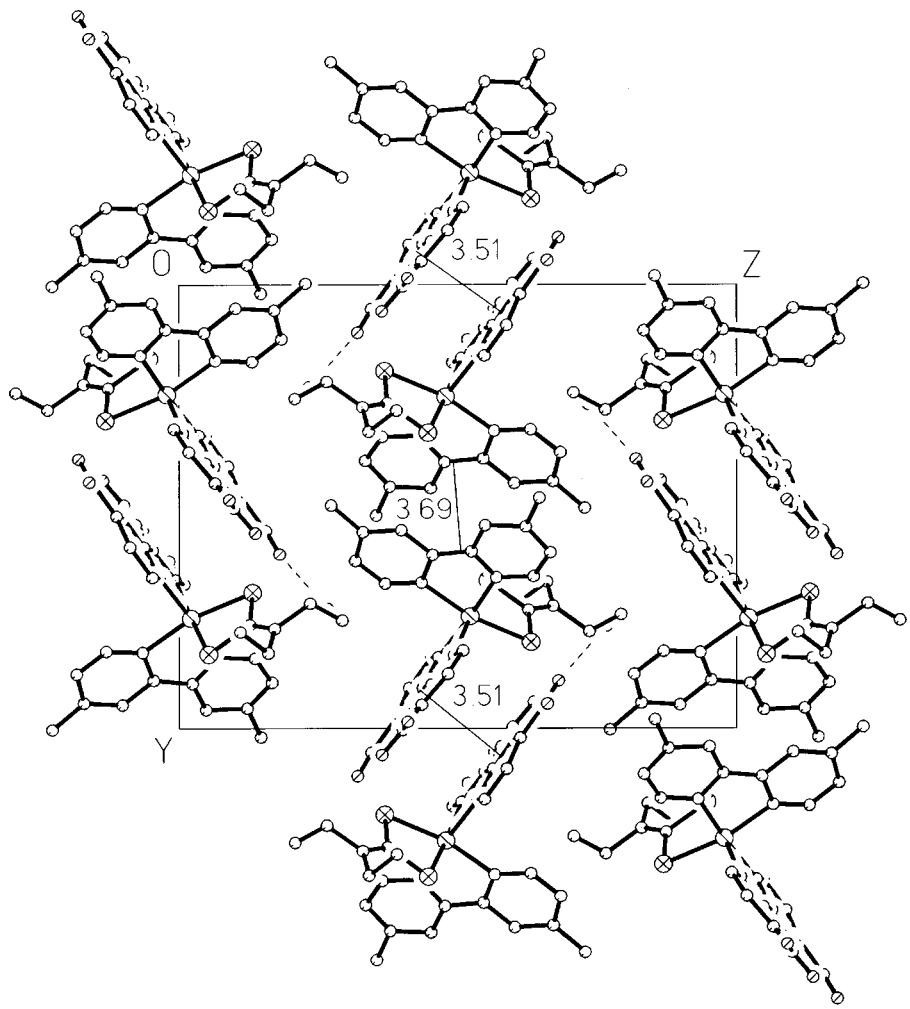

FIG. 2. Crystal structure **3**. The intermolecular π–π-interactions of the bpy ligands (corresponding interplanar separations are given in Å) are connecting molecules **3** into the chains parallel to the *b*; the hydrogen bonds O–H … O between the chains lead to the formation of layers, parallel to the *ab* plane.

TABLE 5

Intermolecular Contacts (Å) of Non-Hydrogen Atoms in Crystal Structure 3[a] and Characteristic Bond Angles in the Possible Hydrogen Bonds

O(31)···O(42)($x-1$, y, z)	3.20(3)[b]	C(36)O(31)O(42)	141.6(8)
		C(46)O(42)O(31)	131.4(8)
O(31)···C(4)($-x$, $-y$, $1-z$)	3.14(5)		
O(32)···O(42)($-x$, $1/2-y$, $z-1/2$)	2.43(3)[b]	C(32)O(32)O(42)	120.7(2)
		O(32)O(42)C(46)	131.4(8)
O(32)···C(44)($x-1$, y, z)	3.09(4)		
O(41)···C(14)(x, $y-1/2$, $3/2-z$)	3.20(3)		
O(41)···O(1W)(x, y, $z+1$)	2.89(4)[b]	C(46)O(41)O(1W)	107.5(8)
O(42)···C(36)($x+1$, y, z)	3.22(4)		
C(31)···C(42)($-x$, $-y$, $1-z$)	3.33(3)		
C(35)···C(46)(($-x$, $-y$, $1-z$)	3.29(3)		
O(1W)···C(24)($-x$, $-y$, $-z$)	3.32(4)[b]	O(1W)C(24)C(25)	90.1(9)

[a]Comprises contacts, which are shorter as corresponding sums of van der Waals radii O + C = 3.32 Å and C + C = 3.40 Å (23).

[b]Hydrogen bond.

the extended along the *y* axis chains of complex molecules **3**, associated via the intermolecular π–π-interactions of the bipyridine (bpy) ligands (Fig. 2). The π-interaction of the HOOC-substituted bpy ligands proceeds around the inversion center at (0, 0, 1/2), the H_3C-substituted bpy ligands interact around the inversion center (1/2, 1/2, 1/2). In the chains, the HOOC-substituted bpy ligands interact stronger, as the H_3C-substituted ligands (the interplanar separations of *p*-systems of bpy ligands are 3.51 and 3.69 Å, respectively). Similar intramolecular π–π-interactions of bipyridine ligands were found in the crystals of [(2,2′-bpy)(NCS)]$_2$Ru(II) (**4**, solvate with CH_3CN) (19) and [(4,4′-di-(MeO)-2,2′-bpy)$_3$Fe(II)(PF$_6$)$_2$] (**5**) (20). The hydrogen bonds between the carboxylate groups (Table 5) leads further to the association of chains of complex molecules **3** into the sheets parallel to the *ab* plane of crystal **3**.

Each molecule within one layer of crystal **3** is surrounded by four other mutually centrosymmetrically related antiparallel head-to-tail oriented molecules of **3**. Hence, the layers of complexes in crystal **3** (like the layers of complexes Ru(etcbpy)$_2$(NCS)$_2$ in crystal **1**) cannot be used as a simple model for a positioning of sensitizer molecules **3** on the polar surface of TiO_2 nanocrystals. In contrast to crystals **1** and **3**, the polar neighboring molecules are oriented in crystal **2a** parallel and arranged into the layers, which are parallel to the *ab* plane of the crystal **2a** (Fig. 3) (8). Two layers of molecules **2a** together with "inorganic" layer,

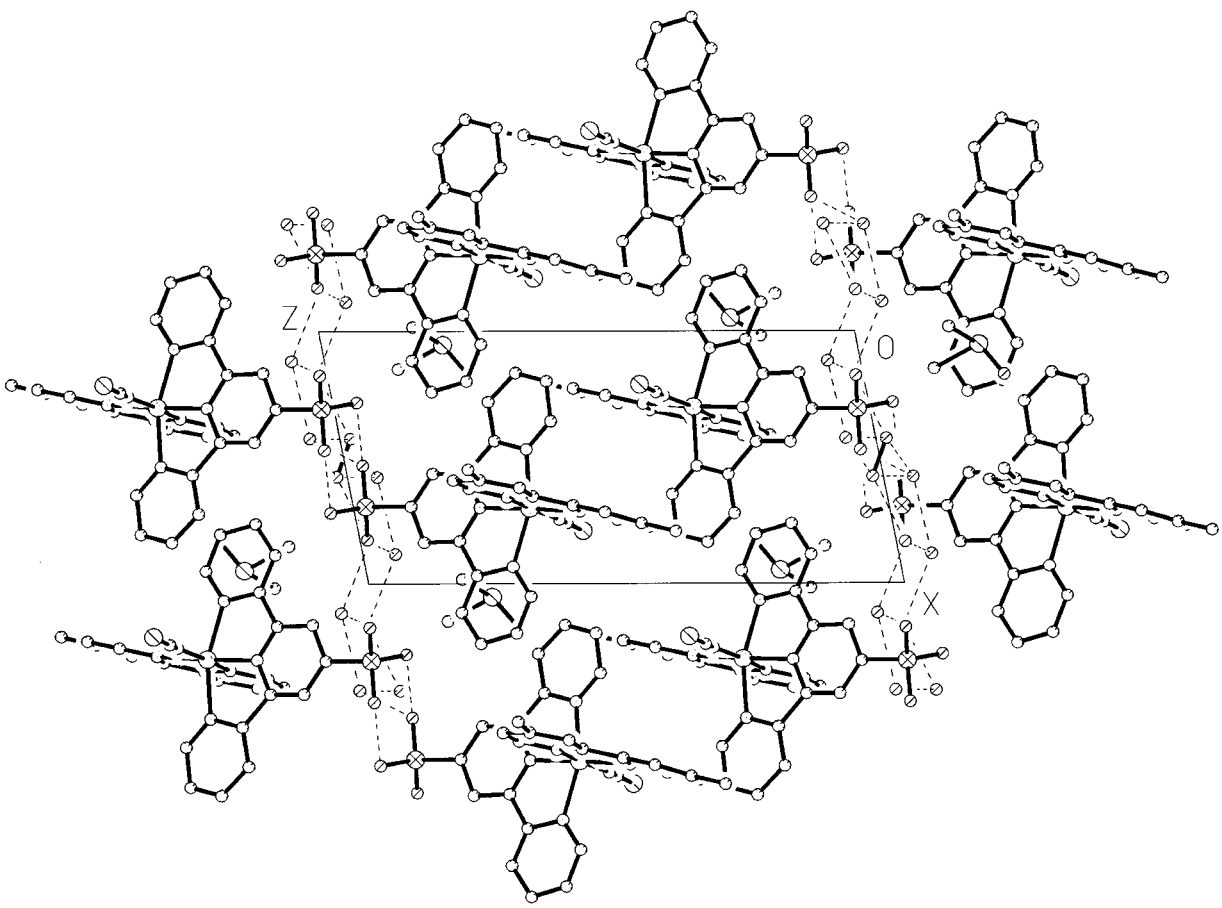

FIG. 3. Cumulated bilayers in crystal **2a** (*ac* projection of the crystal is shown; the O–H … O hydrogen bonds are shown by dotted lines).

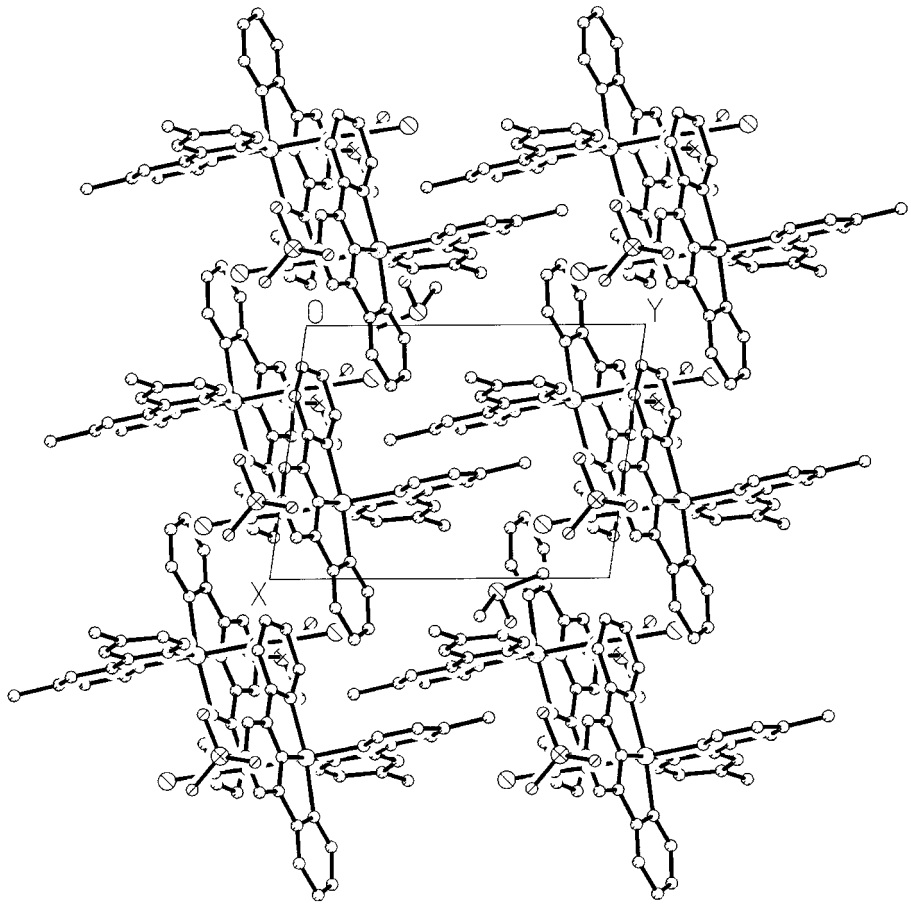

FIG. 4. The orientation of the molecules to the *ab* plane of crystal **2a**. This projection represents the model of anchoring of sensitizer **2** to the semiconductor surface.

consisting of O atoms of the groups $-P(=O)(O^-)(OH)$ and crystallization water molecules are forming a so-called cumulated bilayer (4, 21), the outer surfaces of which are covered by hydrophobic sides of the bpy ligands. The hydrogen bonds with the participation of the O atoms of terminal phosphonic groups are the driving force of the formation cumulated bilayers in crystal **2a**. The parallel tail-to-tail orientation of the neighboring molecules allows the use of the structure of the layer in crystal **2a** as a model for the anchoring of sensitizer **2a**, formed as the monolayer on the semiconductor surface (Fig. 4).

Sensitizer **1** shows C_2 symmetry and it can anchor to the flat semiconductor in eight possible ways: the number of $-COO^-$ groups, varying from 1 to 4, and the number of surface areas, varying from 97 to 130 $Å^2$, (Table 6). The surface area of complex **2a** on the *ab* plane of crystal **2a** is $(a \times b \times \sin g) = 98.92\ Å^2$, but may be further decreased during anchoring, because (a) the main molecular axes of complex **2a** are not normal to the *ab* plane of crystal **2a** (lines Ru ⋯ P are forming with the *ab* plane angle of 39.3°, the dihedral angle between the plane of three atoms O(1), O(2), and O(3) of the phosphonic group $P(=O)(O^-)(OH)$, and the *ab* plane is 35.0° (Fig. 3)) and (b) the orthogonal orientation of bpy and terpy ligands in crystal **2a** allows more dense packing of the sensitizer molecules within the monolayer on the semiconductor surface (Fig. 5). The surface area of the molecule of sensitizer **3** varies from 104 to 128 Å, depending on the number of anchoring carboxylate groups and orientation of molecule to the surface (Fig. 6).

Figure 7a shows the SEI pattern obtained from the (001) surface of the specimen. The bright areas are produced by enhanced electron intensities within the polar angle of 52° and, therefore, represent internuclear directions within this cone in a near-surface region of the crystal whose thickness is determined by the inelastic mean free path of electrons at 2 keV. This quantity is approximately 20 Å (14). The near-perfect contrast quality of the pattern, which is obtained from the crystal without any cleaning process of the surface, leads to the conclusion that structurally damaged surface layers are confined to a very thin region layer of the surface. The striking feature of the pattern is the fourfold symmetric

TABLE 6
Surface Areas of Sensitizers 1, 2a, and 3, Projected on the Flat (Semiconductor) Support, for Different Types of Anchoring

Sensitizer	N^a	Surface area (Å^2)^b	Sensitizer	N^a	Surface area (Å^2)^b	Anchoring group^c
1	1	121	**3**	1	128	C(36)
	2	97–130^d		1	104	C(46)
	3	127		2	108	C(36), C(46)
	4	130				
2a	1	86				

Note. See also Fig. 6.

[a] Number of anchoring groups.

[b] The surface area analysis was performed on a Power Macintosh 7100 computer using the public domain NIH Image program (developed at the U.S. National Institutes of Health and available from the Internet by anonymous FTP from zippy.nimh.nih.gov or on floppy disk from the National Information Service, Springfeld, Virginia, part No. PB95-500195GEI).

[c] Only the numbers of ipso-atoms of carboxy-groups are given.

[d] Depending on the anchoring (3).

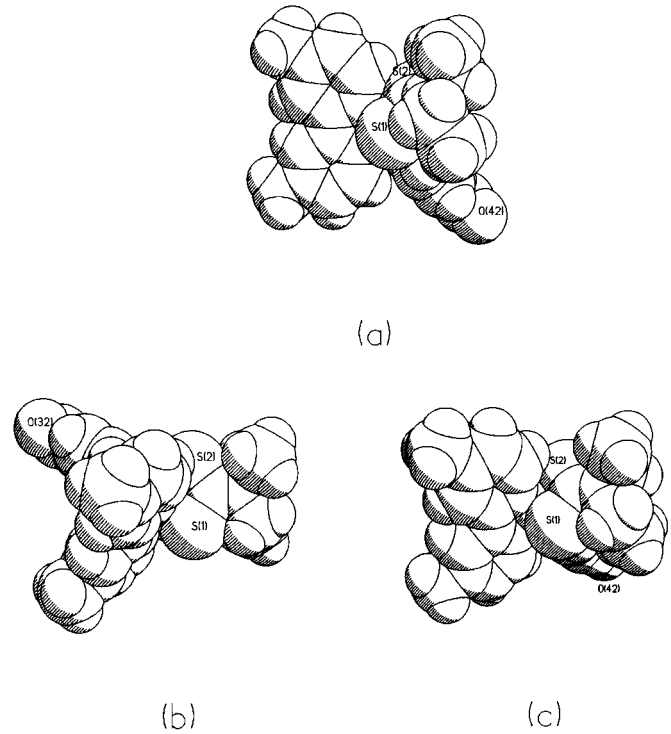

FIG. 6. Three types of the anchoring of sensitizer **3** to the flat semiconductor surface via one carboxylate group at atoms C(36) (a) and C(46) (b) and two carboxylate groups at atoms C(36) and C(46) (c).

alignment of the bright patches, as expected from the (001) surface. The bright cross, which dominated the pattern, is produced by closely spaced internuclear directions and, therefore, is an indication of an atomically dense unit cell. The contrast details of the SEI pattern are interpreted in terms of a central projection of the vectors connecting the next-neighbor atoms with a reference atom. The results of the computer generation of all vectors within the observable cone of 52° for the (001) surface of the anatase is shown in Fig. 7b. The relative bright spots on the branches of the cross, located at polar angles of ca. 22° and 39° (Fig. 7a), may be identified as the [101] and [201] directions. The horizontal branch of the cross represents the (010) plane, while the vertical one is formed by the (100) and all other parallel to them. Four additional bright spots, arranged in fourfold symmetry at a polar angle of ca. 29°, are assigned to the [111] direction.

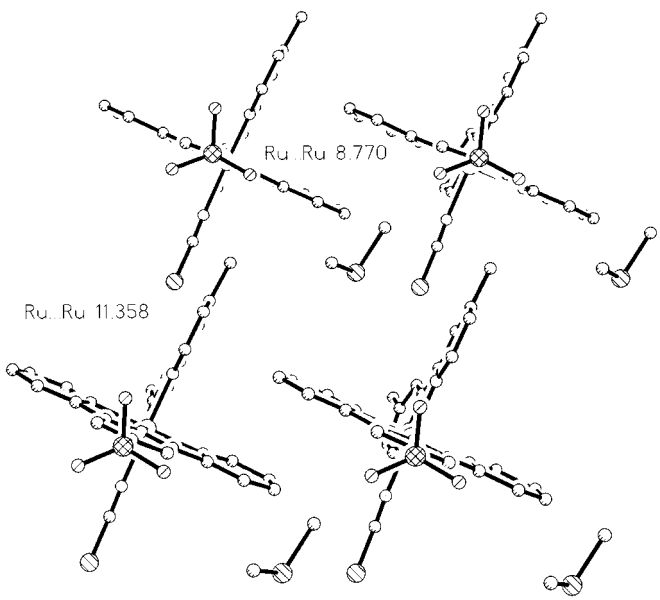

FIG. 5. Projection of crystal structure **2a** on the plane of the three oxygen atoms of the group –P(=O)(O$^-$)(OH). Crystallization water molecules are not shown. The Ru ··· Ru separations (Å) in crystal **2a** are given.

A more realistic simulation of SEI pattern requires a wave-mechanical calculation. A multiple-scattering treatment of the problem is only available for the low electron energies (10), but not for high energies relevant for the SEI. Therefore, we have used a single-scattering model invoking the SSC approximation (15) for the simulation of the intensities observed for the SEI from the (001) face of anatase. The calculated intensities (Fig. 7c) show excellent agreement with the experimental data. Therefore, we conclude that the crystalline structure of the naturally grown anatase specimen is flawless in a near-surface region examined by SEI and that there is no detectable reconstruction of the surface layers.

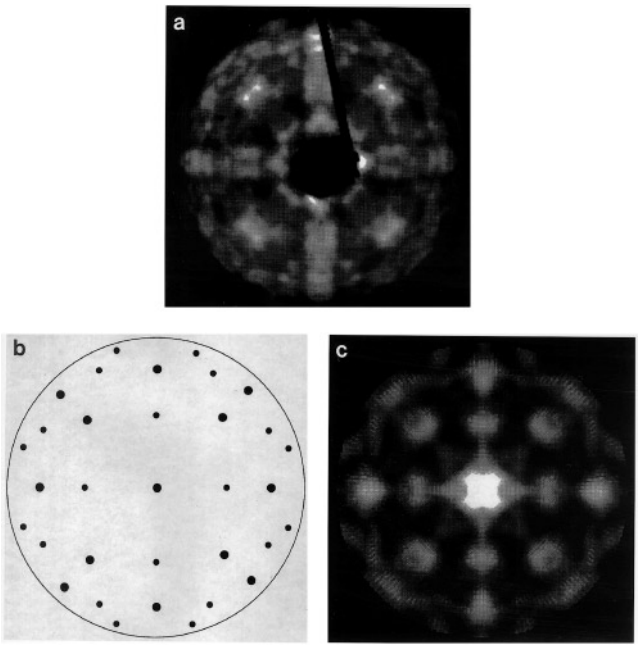

FIG. 7. Comparison of experimentally observed and calculated patterns for the (001) surface of the anatase single crystal. (a) A secondary-electron pattern obtained at 2000 eV with the primary-electron beam directed along the [001] direction of the tetragonal anatase single crystal. The central portion of the image is covered by the electron gun used for the excitation. Bright spots are identified as originating from atoms along the [101], [201], and [111] directions. (b) A calculated central projection of the anatase structure. The observable directions are indicated by filled circles. Overlapping directions are presented by larger circles. The bulk atomic positions were assumed to continue up to the surface. (c) Calculated pattern using single-scattering formalism of the SSC model described in the text. The good agreement with the experiment indicates that the (001) surface is not reconstructed.

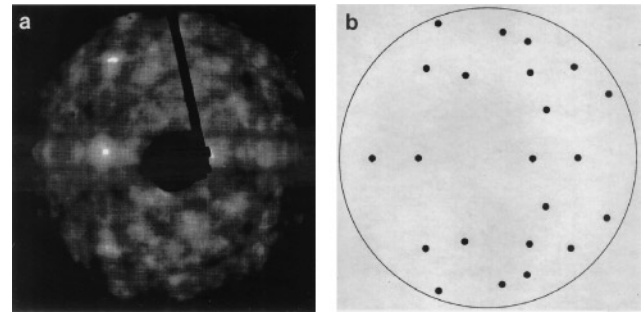

FIG. 8. SEI pattern of the (101) surface of the anatase single crystal. (a) A secondary- electron pattern obtained after rotation the sample around the [010] direction by approximately 68° so that the primary-electron beam is incident along the [101] direction of the crystal. (b) Calculated central projection of the anatse structure for the (101) surface. The good agreement with the experimental pattern verifies that there is no reconstruction of the (101) surface.

The dominant physical process responsible for the image formation in SEI is electron-atom scattering. Decreasing the energy from 2000 to 400 eV causes electron scatter at the periodic potential of the surface atom and one obtains sharp diffraction patterns characteristic of the reciprocal lattice. This is the LEED regime where the surface sensitivity is enhanced, and any deviation from a perfect surface structure can readily be observed. Around 400–500 eV, the (001) surface of anatase shows LEED patterns typical for the surface with fourfold symmetry without reconstruction. The angular positions of the diffraction spots indicate a periodicity of $3.7 + 0.2$ Å in perfect agreement with the nearest-neighbor distance in the (001) plane 3.785 Å expected from the bulk structure. At energies lower than 400 eV, where the surface sensitivity of LEED is further increased, diffraction spots are obliterated. This indicates submonolayer-thin contamination of the "as-received" (001) anatase surface.

In the SEI pattern in Fig. 8a, the horizontal plane is (010) of the anatase crystal. The primary electron beam is now incident along the [101] direction which coincides with the center of the display unit. Twofold symmetry, characteristic of the (101) surface of the tetragonal anatase crystal, is apparent in Fig. 8a. A bowed cross is located on the left-hand side, where the bright patch in its center at a polar angle of approximately 22° represents the [100] direction. Further to the left on the (010) plane, at a polar angle of approximately 44°, the [101] direction is discernible. The bowed vertical branch of the cross contains directions lying in the (001) and above (below) the plane (010); at a distance of approximately 27° and 45° from [100], the [210] ([$\bar{2}$10]) and [110] ([$\bar{1}$10]) directions could be observed.

The good agreement with the experiment for the computed directions for the (101) surface (Fig. 8b) leads to the conclusion that the positions of the surface atoms do not deviate from the bulk values; i.e., the surface structure is near perfect and not reconstructed within ca. 20 Å. Yet, at lower electron energies no LEED pattern could be observed from the (101) surface indicating that the top atomic layer is disordered and/or contaminated. However, the good contrast quality of the SEI pattern, shown in Fig. 8a, confirms that this layer is not thicker as one monolayer.

In an attempt to produce atomically clean surface which would result in LEED pattern at low electron energies, we have applied mild sputtering to both the (001) and the (101) surfaces (Fig. 9). As a result of this treatment, all bright patches have disappeared (cf. Fig. 7a), and electron densities are concentrated in bright bands corresponding to the (100), (110), and (010) planes. This observation can be interpreted as an obliteration of atom positions, yet preserving the average structure of the crystal. The (101) surface changes in a similar way. In order to examine whether this structural change is caused by an oxygen deficiency in the structure which has a higher sputter yield than Ti (23), we exposed

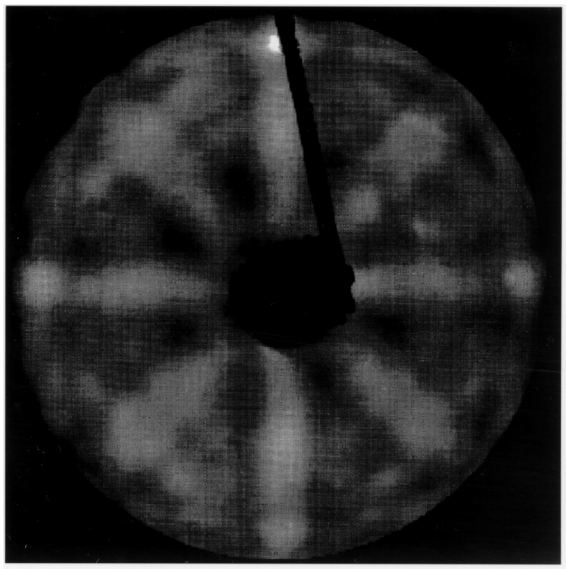

FIG. 9. SEI pattern obtained from the (001) surface after a mild sputtering with He^+ ions for 15 minutes (500 eV, 1 $\mu A \cdot mm^{-2}$). The bright patches that represent interactomic vectors, as shown in Fig. 6a, are all replaced by bright bands that characterize low-index atomic planes.

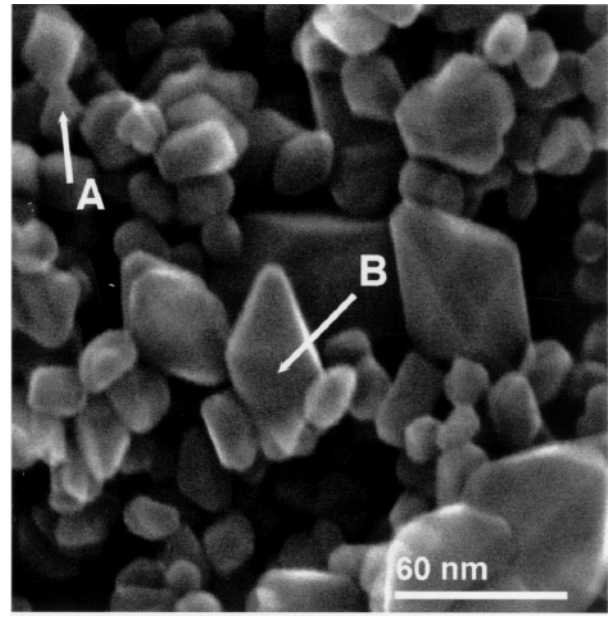

FIG. 10. Scanning electron micrograph of the colloidal TiO_2 anatase film. The nanocrystals terminated mostly by the (101) and (001) faces, e.g., nanocrystals A and B. The possible amounts of the sensitizer molecules on the mostly exposed faces may be estimated using the data on the surface areas of sensitizer molecules (Table 6).

both surfaces to oxygen. Introducing oxygen into the vacuum system up to 1000 L (1 L = 1 $\mu Torr \cdot sec$) did not produce any effect, and the contrast details in the original SEI pattern could not be restored. Considering that sputtering was extremely mild, we concluded that TiO_2 anatase has a very sensitive structure owing to the fact that both Ti and O are light elements. Yet, it is interesting to observe that a naturally grown crystal has an atomic perfection that is at

TABLE 7
Interplanar Separations *d* (Å) and Intensities *I* of Reflections *hkl*, Calculated from Single Crystal data for 2a and Recorded for Powder 2b[a]

Phase **2a**										Phase **2b**									
h	*k*	*l*	*I*	*d*	*h*	*k*	*l*	*I*	*d*	*h*	*k*	*l*	*I*	*d*	*h*	*k*	*l*	*I*	*d*
0	0	1	3	17.46	0	2	1	49	5.08	2	1	0	11	3.81	0	0	1	84	10.13
0	1	0	68	11.14	0	−2	2	18	5.07	2	0	2	11	3.58	−1	0	1	69	9.54
0	1	1	42	8.78	1	1	2	6	4.66	1	−3	1	13	3.58	1	0	1	54	8.38
0	0	2	11	8.73	1	0	3	31	4.44	−2	−1	3	36	3.57	0	1	0	100	7.83
−1	0	1	38	8.33	1	2	0	28	4.39	2	−2	1	12	3.54	−2	0	1	36	7.42
0	−1	2	26	7.47	0	−2	3	22	4.38	0	−1	5	14	3.49	3	0	0	33	6.22
−1	1	0	22	7.31	0	0	4	8	4.37	2	0	3	12	3.17	−3	0	1	49	5.71
1	0	1	37	7.17	0	−1	4	24	4.30	−1	−2	5	13	3.08	4	0	0	39	4.69
−1	0	2	32	6.78	−1	2	2	100	4.29	0	−3	4	13	3.08	−4	0	1	80	4.53
0	0	3	27	5.82	2	0	0	29	4.28	−1	3	3	17	2.96	−1	1	2	34	4.27
−1	−1	2	19	5.81	−2	1	1	11	4.20	−3	−1	2	11	2.72	−1	0	3	28	3.42
−1	1	2	33	5.77	−2	0	2	12	4.16	−1	−4	3	14	2.41	3	2	0	42	3.31
1	1	1	40	5.58	2	0	1	44	3.98						2	0	3	23	3.05
0	−1	3	27	5.53	−2	−1	1	11	3.91										

[a] The *d* values in the range of $2\Theta = 5$–42° are given. The unit cell constants for the **2a** phase are: $a = 8.770(1)$, $b = 11.358(3)$, $c = 17.945(5)$ Å, $\alpha = 97.72(2)$, $\beta = 99.76(2)$, $\gamma = 96.73(2)^\circ$, $V = 1727.6(8)$ Å^3 (composition of crystal **2a** is $\mathbf{2} \cdot (CH_3)_2SO \cdot 3.5H_2O$). The powder pattern of **2b** was indexed using TREOR program in monoclinic unit cell with $a = 18.97(2)$, $b = 7.800(8)$, $c = 10.282(7)$ Å, $\beta = 98.52(9)^\circ$, $V = 1504.4$ Å^3 (the broad peaks at $2\Theta = 13.06$ and 22.52° were not used for indexing).

least comparable to those of artificially grown crystals, a general occurrence in oxygen-containing minerals. A mild heat treatment at 500 K had no effect on the SEI pattern shown in Fig. 9. A treatment at higher temperatures was not attempted in order to avoid a possible phase transformation of the crystal and/or a cracking of the large crystal along the planes that might possibly contain gas impurities embedded into the structure during the growth process in nature. While the surface structure of the TiO_2 rutile was studied extensively, see, e.g., (24–27), we believe that the present results are the first ones on anatase.

The amounts of sensitizer molecules on the mostly exposed faces of anatase nanocrystals may be estimated for the given nanocrystal sizes in the anatase electrodes, using the surface areas of sensitizers **1**, **2a**, and **3**, calculated for space filling models of **1**, **2a**, and **3** using van der Waals radii of the atoms of sensitizers (see Table 6).

The anatase nanocrystals in thin colloidal TiO_2 films are terminated mostly by the (101) and (001) faces (3) (Fig. 10). Two HRTEM patterns of the carefully prepared (101) cut anatase single crystal sample, coated with sensitizer **2b** (obtained as ethanol solution), are shown in Fig. 11. Besides the (101) anatase fringes, the appearance of moire patterns due to overlapping of thin sensitizer **2b** crystals with anatase (101) fringes could be seen, with the moire periodicities of $D_M = 14.54$ Å in Fig. 11a and $D_M = 9.96$ Å in Fig. 11b. The calculated for pattern 11a d(**2b**) ≈ 4.51 Å agrees quite well with the $d(-401) = 4.53$ Å for powder **2b** and close to the strongest peak of $d(-122) = 4.29$ Å for single crystal **2a**, as one may see from the Table 7 and Fig. 12, where the powder diffraction patterns are compared for phases **2a** (calculated from single crystal data) and **2b** (recorded). As one may see from Fig. 13, planes (−122) of crystal **2a** comprise molecules with the orientation, advantageous for the anchoring to the semiconductor surface via –P(O)(OH)(O^-). The separations with $d \approx 3.68$ Å, calculated for the moire pattern in Fig. 11b, do not coincide with any lattice separation of the powder **2b**, but are close to

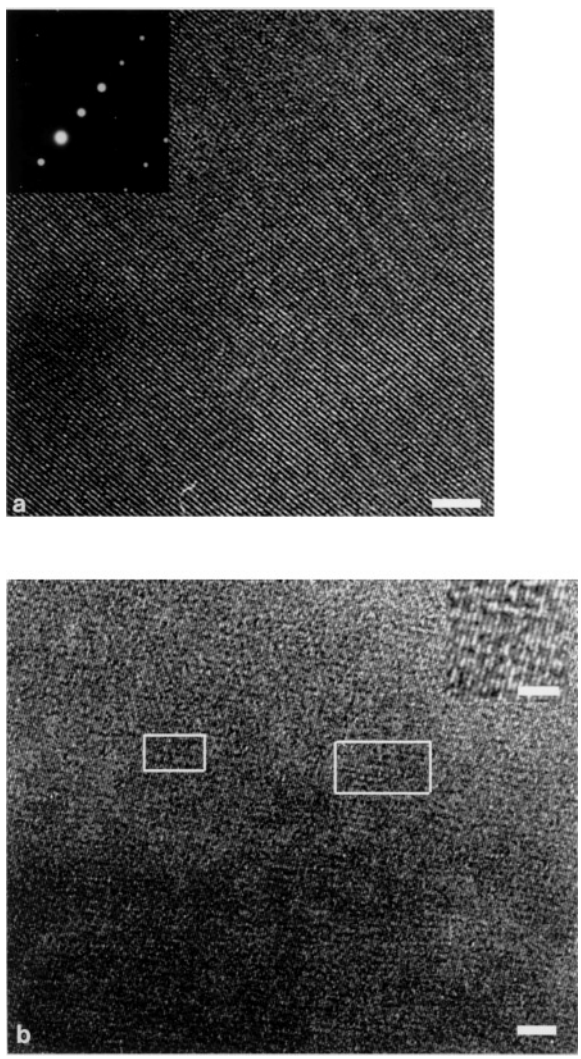

FIG. 11. HRTEM images (a) and (b) of the (101) face of anatase single crystal ($a = 3.7892(4)$, $c = 9.537(1)$ Å (26)), coated with sensitizer **2b**. Only the (010) lattice separations of the anatase could be seen, $d(010) = 3.63$ Å for (a) and 3.53 Å for (b). The moire spacings are $D_M = 14.54$ Å (a) and 9.96 Å (b). Scale bars are 3 nm on (a) and 5 and 2.5 nm (magnified fragment) on (b).

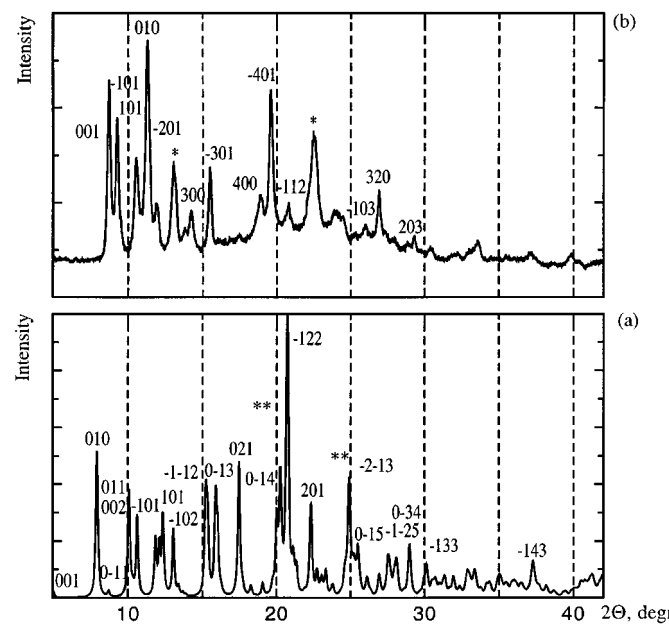

FIG. 12. Comparison of the powder diffraction pattern, recorded for powder **2b** (a) with calculated from the single crystal data powder diffraction pattern of phase **2a** (b). Phase **2a** was crystallized from DMSO; **2b** was crystallized from acetonitrile. *Broad peaks at $2\Theta = 13.06$ and 22.52° in pattern **2b** were not included in the indexing of the pattern with TREOR program. **The $d(-122)$ and $d(-2-13)$ separations of powder pattern **2a**, close to separations of **2b** thin crystal, calculated from moire patterns in Fig. 11.

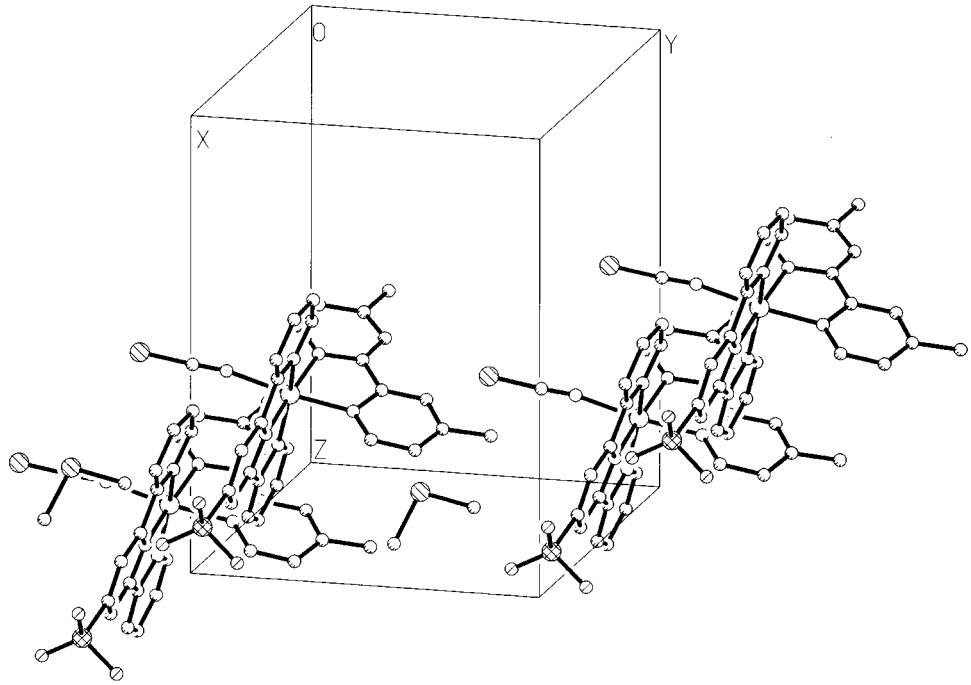

FIG. 13. Projection of crystal structure **2a** on plane (−122). The vectors of bonds Ru ⋯ P(=O)(OH)(O^-) are oriented advantageous for the anchoring to the semiconductor surface, which is approximately parallel to plane *ab* of cumulated bilayers in crystal **2a** (see also Figs. 3 and 4).

the strong peak $d(-2-13) = 3.57$ Å of powder pattern of **2a**. The formation of different crystal modifications of sensitizer **2** on the anatase surface may be supposed. Planes (−2 − 13) also comprise molecules **2**, properly oriented for the interaction with the semiconductor surface through the –P(O)(OH)(O^-) groups.

CONCLUSION

The X-ray single crystal study of three new efficient sensitizers was used for (a) modeling the structure of two-dimensional sensitizer coatings. This produced especially clear results for the crystal of the phosphonated sensitizer **3**, whose molecules are forming parallel head-to-head packing. (b) The estimation of the surface areas of the sensitizer for different types of anchoring to the semiconductor surface, which depend on the number and molecular position of the anchoring groups. The LEED study of naturally grown anatase single crystals at the electron energies of 30–500 eV shows submonolayer-thin contamination of both mostly exposed (001) and (101) surfaces. At the same time, the SEI study using the electron energies near 2000 eV does not indicate detectable surface reconstruction of these anatase faces. The moire patterns due to overlapping of thin sensitizer crystal with the anatase (101) fringes are observed on HRTEM images of anatase single crystal coated with phosphorylated Ru sensitizer. Planes (−122) and (−103) may describe the orientation of sensitizer molecules to (101) planes of anatase support. Using the data obtained on the sensitizer surface areas, the average number of sensitizer molecules on the mostly exposed faces of anatase nanocrystals could be estimated for given nanocrystal size in colloidal anatase film.

ACKNOWLEDGMENTS

The authors are indebted to R. Wessicken for the help in the recording and interpretation of the HRTEM patterns, and to the Swiss Energy Office, Project EF-REN (91)054, and the Swiss Comission for the Encouragement of Scientific Research, Project 2442, for financial support.

REFERENCES

1. M. Grätzel, *Comments Inorg. Chem.* **12,** 93 (1991).
2. P. Pechy, F. Rotzinger, M. K. Nazeeruddin, O. Kohle, S. M. Zakeeruddin, R. Humphry-Baker, and M. Grätzel, *Chem. Commun.* 65 (1995).
3. V. Shklover, M.-K. Nazeeruddin, S. M. Zakeeruddin, C. Barbe, A. Kay, T. Haibach, W. Steurer, R. Hermann, H.-U. Nissen, and M. Grätzel, *Chem. Mater.* **9,** 430 (1997).
4. F. Nüesch, M. Grätzel, R. Nesper, and V. Shklover, *Acta Crystallogr.* **B52,** 277 (1996).
5. J. Pecaut and R. Masse, *Acta Crystallogr.* **B49,** 277 (1993).
6. M. Bagieu-Beucher, R. Masse, and D. Tranqui, *Z. Anorg. Allg. Chem.* **606,** 59 (1991).
7. R. Masse and J. Zyss, *Mol. Eng.* **1,** 149 (1991).

8. S. M. Zakeeruddin, M. K. Nazeeruddin, P. Pechy, F. P. Rotzinger, Humphry-Baker, K. Kalyanasundaram, M. Grätzel, V. Shklover, and T. Haibach submitted for publication.
9. G. Somorjai, "Introduction to Surface Chemistry and Catalysis," p. 48. Wiley, New York, 1994.
10. J. B. Pendry, "Low Energy Electron Diffraction." Academic Press, London, 1974.
11. S. M. Zakeeruddin, M. K. Nazeeruddin, V. Shklover, and M. Grätzel, submitted for publication.
12. CAD4-EXPRESS. User Manual; Delft Instruments, X-Ray Diffraction, Delft, 1992.
13. G. M. Sheldrick, SHELXTL PLUS, VAX/VMS Version, Siemens Analytical X-Ray Instruments Inc., Madison, WI, 1990.
14. M. P. Seah and W. A. Dench, *Surf. Interf. Anal.* **1,** 2 (1979).
15. M. Erbudak, M. Hochstrasser, and E. Wetli, *Mod. Phys. Lett.* **B8,** 1759 (1994).
16. C. S. Fadley, *in* "Synchrotron Radiation Reserach: Advances in Surface Science" (R. Z. Bachrach, Ed.) Plenum, New York, 1990.
17. "Digital Micrograph. Users Guide, 1992–1994." Gatan, Pleasanton, CA.
18. A. W. Cordes and M. Draganjac, *Acta Crystallogr.* **C44,** 363 (1988).
19. R. H. Herber, G. Nan, J. A. Potenza, H. J. Schugar, and A. Bino, *Inorg. Chem.* **28,** 938 (1989).
20. V. Shklover, R. Nesper, S. M. Zakeeruddin, D. M. Fraser, and M. Grätzel, *Inorg. Chim. Acta* **247,** 237 (1996).
21. M. Miyata and K. Miki, *in* "Reactivity in Molecular Crystals" (Y. Ohashi, Ed.), p. 153. VCH, Weinheim/New York, 1993.
22. "Topics in Applied Physics; Sputtering by Particle Bombardement," (R. Benrish, Ed.) Vol. 47. Springer Verlag, New York, 1981.
23. A. Bondi, *J. Phys. Chem.* **68,** 441 (1964).
24. P. W. Murray, F. M. Leisble, H. Muryn, C. F. Fischer, C. F. J. Flipse, and G. Thornton, *Surf. Sci.* **262,** 395 (1992).
25. Y. Gao, Y. Liang, and S. A. Chambers, *Surf. Sci.* **348,** 17 (1996).
26. A. Berko, G. Menesi, and F. Solymosi, *Surf. Sci.* **372,** 202 (1997).
27. M. Horn, C. F. Schwerdtfeger, and E. P. Meagher, *J. Am. Ceram. Soc.* **53,** 124 (1970).